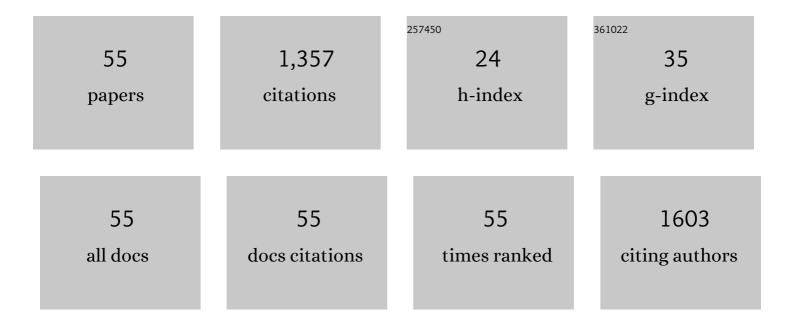
## Iris Yuwen Zhou

List of Publications by Year in descending order

Source: https://exaly.com/author-pdf/4479338/publications.pdf Version: 2024-02-01



#	Article	IF	CITATIONS
1	Dynamic contrast-enhanced magnetic resonance imaging of the lung reveals important pathobiology in idiopathic pulmonary fibrosis. ERJ Open Research, 2021, 7, 00907-2020.	2.6	8
2	Molecular Imaging of Fibrosis. , 2021, , 1447-1468.		0
3	Improving the reactivity of hydrazine-bearing MRI probes for <i>in vivo</i> imaging of lung fibrogenesis. Chemical Science, 2020, 11, 224-231.	7.4	33
4	Collagen-targeted molecular imaging in diffuse liver diseases. Abdominal Radiology, 2020, 45, 3545-3556.	2.1	7
5	Advanced MRI of Liver Fibrosis and Treatment Response in a Rat Model of Nonalcoholic Steatohepatitis. Radiology, 2020, 296, 67-75.	7.3	22
6	Advances in functional and molecular MRI technologies in chronic liver diseases. Journal of Hepatology, 2020, 73, 1241-1254.	3.7	27
7	Determination of multipool contributions to endogenous amide proton transfer effects in global ischemia with high spectral resolution in vivo chemical exchange saturation transfer <scp>MRI</scp> . Magnetic Resonance in Medicine, 2019, 81, 645-652.	3.0	45
8	Preliminary evaluation of dynamic glucose enhanced MRI of the human placenta during glucose tolerance test. Quantitative Imaging in Medicine and Surgery, 2019, 9, 1619-1627.	2.0	8
9	In vivo microscopic diffusional kurtosis imaging with symmetrized double diffusion encoding EPI. Magnetic Resonance in Medicine, 2019, 81, 533-541.	3.0	10
10	JOURNAL CLUB: Evaluation of Diffusion Kurtosis Imaging of Stroke Lesion With Hemodynamic and Metabolic MRI in a Rodent Model of Acute Stroke. American Journal of Roentgenology, 2018, 210, 720-727.	2.2	24
11	pHâ€sensitive amide proton transfer effect dominates the magnetization transfer asymmetry contrast during acute ischemia—quantification of multipool contribution to in vivo CEST MRI. Magnetic Resonance in Medicine, 2018, 79, 1602-1608.	3.0	43
12	A generalized ratiometric chemical exchange saturation transfer (CEST) MRI approach for mapping renal pH using iopamidol. Magnetic Resonance in Medicine, 2018, 79, 1553-1558.	3.0	57
13	Longitudinal Assessments of Normal and Perilesional Tissues in Focal Brain Ischemia and Partial Optic Nerve Injury with Manganese-enhanced MRI. Scientific Reports, 2017, 7, 43124.	3.3	10
14	Progress toward quantitative in vivo chemical exchange saturation transfer (CEST) MRI. Israel Journal of Chemistry, 2017, 57, 809-824.	2.3	12
15	Quantitative chemical exchange saturation transfer (CEST) MRI of glioma using Image Downsampling Expedited Adaptive Least-squares (IDEAL) fitting. Scientific Reports, 2017, 7, 84.	3.3	65
16	Direct saturation orrected chemical exchange saturation transfer MRI of glioma: Simplified decoupling of amide proton transfer and nuclear overhauser effect contrasts. Magnetic Resonance in Medicine, 2017, 78, 2307-2314.	3.0	18
17	pH imaging reveals worsened tissue acidification in diffusion kurtosis lesion than the kurtosis/diffusion lesion mismatch in an animal model of acute stroke. Journal of Cerebral Blood Flow and Metabolism, 2017, 37, 3325-3333.	4.3	32
18	Simultaneous spinâ€echo and gradientâ€echo BOLD measurements by dynamic MRS. NMR in Biomedicine, 2017, 30, e3745.	2.8	2

#	Article	IF	CITATIONS
19	A theoretical analysis of chemical exchange saturation transfer echo planar imaging (CESTâ€EPI) steady state solution and the CEST sensitivity efficiencyâ€based optimization approach. Contrast Media and Molecular Imaging, 2016, 11, 415-423.	0.8	33
20	pH-sensitive MRI demarcates graded tissue acidification during acute stroke ― pH specificity enhancement with magnetization transfer and relaxation-normalized amide proton transfer (APT) MRI. NeuroImage, 2016, 141, 242-249.	4.2	65
21	Fast diffusion kurtosis imaging (DKI) with Inherent COrrelationâ€based Normalization (ICON) enhances automatic segmentation of heterogeneous diffusion MRI lesion in acute stroke. NMR in Biomedicine, 2016, 29, 1670-1677.	2.8	12
22	Tissue Characterization with Quantitative High-Resolution Magic Angle Spinning Chemical Exchange Saturation Transfer Z-Spectroscopy. Analytical Chemistry, 2016, 88, 10379-10383.	6.5	10
23	Organization of the intrinsic functional network in the cervical spinal cord: A resting state functional MRI study. Neuroscience, 2016, 336, 30-38.	2.3	32
24	A method for accurate pH mapping with chemical exchange saturation transfer (CEST) MRI. Contrast Media and Molecular Imaging, 2016, 11, 195-202.	0.8	35
25	Comparison of image sensitivity between conventional tensorâ€based and fast diffusion kurtosis imaging protocols in a rodent model of acute ischemic stroke. NMR in Biomedicine, 2016, 29, 625-630.	2.8	19
26	Structural and Functional Brain Remodeling during Pregnancy with Diffusion Tensor MRI and Resting-State Functional MRI. PLoS ONE, 2015, 10, e0144328.	2.5	22
27	Susceptibility weighted imaging of stroke brain in response to normobaric oxygen (NBO) therapy. , 2015, , .		Ο
28	Quantitative chemical exchange saturation transfer (qCEST) MRI – omega plot analysis of RFâ€spilloverâ€corrected inverse CEST ratio asymmetry for simultaneous determination of labile proton ratio and exchange rate. NMR in Biomedicine, 2015, 28, 376-383.	2.8	48
29	Quantification ofin vivopH-weighted amide proton transfer (APT) MRI in acute ischemic stroke. , 2015, ,		Ο
30	Dietary supplementation with n-3 fatty acids from weaning limits brain biochemistry and behavioural changes elicited by prenatal exposure to maternal inflammation in the mouse model. Translational Psychiatry, 2015, 5, e641-e641.	4.8	51
31	Simplified correction of B <sub>1</sub> inhomogeneity for chemical exchange saturation transfer (CEST) MRI measurement with surface transceiver coil. Proceedings of SPIE, 2015, , .	0.8	Ο
32	Resting-State fMRI Using Passband Balanced Steady-State Free Precession. PLoS ONE, 2014, 9, e91075.	2.5	1
33	Effect of diffusion time on liver DWI: An experimental study of normal and fibrotic livers. Magnetic Resonance in Medicine, 2014, 72, 1389-1396.	3.0	12
34	In vivo visuotopic brain mapping with manganese-enhanced MRI and resting-state functional connectivity MRI. NeuroImage, 2014, 90, 235-245.	4.2	30
35	The inferior colliculus is involved in deviant sound detection as revealed by BOLD fMRI. NeuroImage, 2014, 91, 220-227.	4.2	29
36	Brain resting-state functional MRI connectivity: Morphological foundation and plasticity. NeuroImage, 2014, 84, 1-10.	4.2	52

IRIS YUWEN ZHOU

#	Article	IF	CITATIONS
37	Longitudinal metabolic changes in the hippocampus and thalamus of the maternal brain revealed by proton magnetic resonance spectroscopy. Neuroscience Letters, 2013, 553, 170-175.	2.1	7
38	Functional magnetic resonance imaging of sound pressure level encoding in the rat central auditory system. Neurolmage, 2013, 65, 119-126.	4.2	21
39	Noninvasive fMRI Investigation of Interaural Level Difference Processing in the Rat Auditory Subcortex. PLoS ONE, 2013, 8, e70706.	2.5	17
40	MR Diffusion Tensor Imaging Detects Rapid Microstructural Changes in Amygdala and Hippocampus Following Fear Conditioning in Mice. PLoS ONE, 2013, 8, e51704.	2.5	40
41	Balanced steadyâ€state free precession fMRI with intravascular susceptibility contrast agent. Magnetic Resonance in Medicine, 2012, 68, 65-73.	3.0	25
42	Magnetic resonance spectroscopy reveals N-acetylaspartate reduction in hippocampus and cingulate cortex after fear conditioning. Psychiatry Research - Neuroimaging, 2012, 204, 178-183.	1.8	23
43	In vivo evaluation of retinal and callosal projections in early postnatal development and plasticity using manganese-enhanced MRI and diffusion tensor imaging. NeuroImage, 2012, 59, 2274-2283.	4.2	57
44	BOLD fMRI investigation of the rat auditory pathway and tonotopic organization. Neurolmage, 2012, 60, 1205-1211.	4.2	43
45	High fidelity tonotopic mapping using swept source functional magnetic resonance imaging. NeuroImage, 2012, 61, 978-986.	4.2	26
46	In vivo chromiumâ€enhanced MRI of the retina. Magnetic Resonance in Medicine, 2012, 68, 1202-1210.	3.0	17
47	BOLD responses in the superior colliculus and lateral geniculate nucleus of the rat viewing an apparent motion stimulus. NeuroImage, 2011, 58, 878-884.	4.2	35
48	In vivo retinotopic mapping of superior colliculus using manganese-enhanced magnetic resonance imaging. Neurolmage, 2011, 54, 389-395.	4.2	56
49	Metabolic changes in visual cortex of neonatal monocular enucleated rat: a proton magnetic resonance spectroscopy study. International Journal of Developmental Neuroscience, 2011, 29, 25-30.	1.6	21
50	BOLD Temporal Dynamics of Rat Superior Colliculus and Lateral Geniculate Nucleus following Short Duration Visual Stimulation. PLoS ONE, 2011, 6, e18914.	2.5	34
51	Reduced transverse relaxation rate (RR2) for improved sensitivity in monitoring myocardial iron in thalassemia. Journal of Magnetic Resonance Imaging, 2011, 33, 1510-1516.	3.4	7
52	In vivo manganese-enhanced MRI and diffusion tensor imaging of developing and impaired visual brains. , 2011, 2011, 7005-8.		4
53	In vivo MRI study of the visual system in normal, developing and injured rodent brains. , 2010, 2010, 5689-92.		2
54	Functional MRI of postnatal visual development in normal and hypoxic–ischemic-injured superior colliculi. NeuroImage, 2010, 49, 2013-2020.	4.2	47

#	Article	IF	CITATIONS
55	Functional MRI of postnatal visual development in normal rat superior colliculi. , 2009, 2009, 4436-9.		1